Title
Combination of atomic lines and molecular bands for uranium optical isotopic analysis in laser induced plasma spectrometry

Journal
Journal of Radioanalytical and Nuclear Chemistry, 312(1)

ISSN
0236-5731

Authors
Mao, Xianglei
Chan, George C-Y
Choi, Inhee
et al.

Publication Date
2017-04-01

DOI
10.1007/s10967-017-5197-y

Peer reviewed

Journal of Radioanalytical and Nuclear Chemistry

Combination of atomic lines and molecular bands for uranium optical isotopic analysis in laser induced plasma spectrometry

Names of the authors: Xianglei Mao, George C.-Y. Chan*, Inhee Choi†, Vassilia Zorba, Richard E. Russo

Title: Combination of atomic lines and molecular bands for uranium optical isotopic analysis in laser induced plasma spectrometry

Affiliation(s) and address(es) of the author(s): Lawrence Berkeley National Laboratory, Berkeley, CA 94720, USA

(†present address of Inhee Choi: Korea Institute of Nuclear Safety, 62 Gwahakro, Yuseong-gu, Daejeon, South Korea)

E-mail address of the corresponding author: gcchan@lbl.gov

Combination of atomic lines and molecular bands for uranium optical isotopic analysis in laser induced plasma spectrometry

Xianglei Mao, George C.-Y. Chan[*], Inhee Choi[†], Vassilia Zorba, Richard E. Russo

Lawrence Berkeley National Laboratory, Berkeley, CA 94720, USA

[†]*present address: Korea Institute of Nuclear Safety, 62 Gwahakro, Yuseong-gu, Daejeon, South Korea*

Abstract

Through computer simulation on experimentally acquired optical spectra, uranium isotopic analysis by laser ablation molecular isotopic spectrometry (LAMIS) and laser induced breakdown spectroscopy (LIBS) were studied. The use of only one spectral feature, either the strong UO band at 593.55 nm or the nearby U I 593.382 nm line, are similar in precisions (~1.5% in absolute ^{235}U abundances). Precision improves to 0.72% with the use of a group of U atomic lines from 591.6 to 596.5 nm. The use of both molecular bands and atomic lines further advances the precision to 0.42% and compares well with the U II 424.437 nm single-line benchmark (0.48% precision).

Keywords

Optical isotopic analysis; Uranium; Laser ablation molecular isotopic spectrometry; Laser induced breakdown spectroscopy; Isotope shift.

Introduction

The capability to perform direct chemical analysis on any solid sample is one of the distinguishing characteristics of laser-ablation based analysis. Chemical information (both elemental and isotopic) of the sample is contained in the light emitted by the laser-induced plasma and can be readily probed with an optical spectrometer. The technique termed laser induced breakdown spectroscopy (LIBS) involves the measurement of photon emission typically from atoms (i.e., atomic emission spectrometry); in this particular context, the atom can be either charged (i.e., ionized) or as neutral. In contrast, laser ablation molecular isotopic spectrometry (LAMIS) measures the spectra from molecular radicals that are present when the plasma cools. These two spectrometric techniques are very similar in implementation; in fact, they are produced by and can be measured from the same laser pulse.

The choice of utilizing atomic (i.e., LIBS) or molecular (i.e., LAMIS) spectra for a measurement depends on the application. In general, LIBS is used to determine the content of a particular element of interest in the sample (i.e., elemental analysis) whereas LAMIS is employed to evaluate isotopic ratio of a particular element (i.e., isotopic analysis). This simple classification is based on the fact that an atom (or an atomic ion) possesses only electronic energy levels. Isotopic shifts in electronic energy levels (except the very light and heavy elements) are generally too small to be measured inside atmospheric-pressure plasma, in which several line broadening mechanisms are operating. In contrast, because the vibrational and rotational motions of a molecule heavily depend on its reduced mass, the additional vibrational and rotational energy levels in a molecule greatly amplify the isotopic effects on optical spectra. Consequently, isotopic shifts exhibited in molecular spectra may exceed those in atomic spectra by two to three orders of magnitude [1-3], and become readily measurable in an atmospheric-pressure plasma. Isotopic LAMIS signatures from a number of elements, including H, B, C, N, O, Sr and Zr [1-6], have already been reported.

For the very light or heavy elements, LIBS (atomic spectra) can also be used for their isotopic measurements. For light elements, the different masses of isotopes cause a relatively large fractional change in the mass of the atom, which in turn alters the electron motion with respect to the center of gravity of the atoms and hence the associated electronic energy levels. This mass effect is the largest for hydrogen. For instance, the Hα and Hβ lines at 656.464 nm and 486.270 nm are shifted by –174 pm and –130 pm, respectively, for deuterium [7]. For heavy atoms, the large nucleus modifies the electronic energy level of the atom through interactions between the shape and the size of the nuclear charge distribution with the field of the electrons [8, 9]. This field effect is strongest for those electrons that have a finite probability at the origin of the nucleus (i.e., *s*-electrons) [9]. Accordingly, atomic lines of heavy elements (e.g., U) also exhibit appreciable isotope shifts, which can reach tens of picometers [10-12].

Several researchers have reported hydrogen-deuterium analysis by means of LIBS operated under atmospheric pressure [4, 13-16]. Cremers *et al.* [13] also performed isotopic analysis on ^{6}Li and ^{7}Li with LIBS under atmospheric pressure. For heavy elements, uranium has been mostly studied [13, 14, 17, 18]. Doucet *et al.* [14] reported the first study of uranium isotopic analysis with atmospheric pressure LIBS. Although the atomic lines from the two uranium isotopic components were only partially resolved, they demonstrated that isotope ratios can be accurately extracted from the spectra through the use of chemometrics. Cremers *et al.* [13] utilized a spectrometer with a resolution of 75,000, and reported baseline separated isotopic components for the U II 424.437 nm line in atmospheric pressure LIBS. Recently, Morgan *et al.* [17] developed and applied a hybrid interferometric/dispersive spectrometer to measure laser-induced plasma from a metallic uranium foil, and reported that the ^{235}U–^{238}U isotope shift at U II 424.437 nm was resolved in ambient air. We previously performed uranium isotopic analysis in soil matrix with atmospheric-pressure LIBS, and compared the effectiveness of several fitting algorithms to extract isotopic information from the LIBS atomic spectra [18]. LIBS also has been applied to the determination of ^{239}Pu/^{240}Pu isotopic ratios [19], albeit at a reduced pressure of 13.3 kPa.

As LAMIS is a relatively new technique, many of its analytical characteristics have not yet been established. There are three objectives in the present study. Currently, the heaviest element measured with LAMIS for isotopic analysis is Zr ($Z = 40$) [5, 20]. Therefore, the first objective of the present study is to investigate the isotopic spectral features and signal characteristics when LAMIS is applied to a very heavy element like uranium ($Z = 92$). Second, for those elements whose isotopic ratios can be determined with either LIBS or LAMIS, the advantage of one technique over another is largely unknown. So far, there is only one study [4] that compared LIBS and LAMIS side-by-side for isotopic analysis. Sarkar *et al.* [4] assessed both techniques for deuterium/protium ($^2D/^1H$) isotopic ratio determination. The Hα and Dα atomic lines were used for LIBS whereas the OH and OD $A\ ^2\Sigma^+ - X\ ^2\Pi$ molecular bands were utilized for LAMIS [4]. It was concluded that the analytical performances of LAMIS was superior to LIBS for isotopic analysis of hydrogen [4]. Specifically, LAMIS provided an accuracy of 0.5-1.5% compared to 2-5% for LIBS [4]. Although almost all atomic emission lines are broadened by Stark effects inside laser induced plasmas, Stark broadening is particularly pronounced for hydrogen as it is a first-order effect for hydrogen but only second order for other non-hydrogenic atoms [21]. For instance, in the aforementioned LIBS work, the reported line width (full width at half maximum, FWHM) of the Hα atomic line at a gate delay of 10 μs was still 350 pm and was nearly double that of the isotopic shift [4]. However, spectral characteristics for uranium are dramatically different, and it is currently unknown how LAMIS compares with LIBS for isotopic analysis of uranium. Therefore, the second objective of the present work is to assess and compare LAMIS and LIBS for isotopic analysis of uranium. Further, as will be discussed below, emission from U atomic lines and UO molecular bands strongly overlap in time, and spectra acquired at appropriate delay times contain both LIBS and LAMIS signals for U. Understanding the potential of including molecular bands with atomic lines (i.e., a combined LAMIS–LIBS approach) for U isotopic analysis is the third objective of the present study.

Similar to our previous studies [10, 22], experimentally determined measurement characteristics, including noise amplitude and distribution, signal strength, and signal-to-

background ratio were incorporated into the simulation model. The ^{235}U and ^{238}U LAMIS–LIBS spectral profiles used in the simulation were also determined experimentally. It should be stressed that, as the simulation does not include all sources of uncertainties and factors that are present in a real analysis, the analytical figure of merit from simulation represents only the theoretical limit under an idealized situation, and does not reflect what can be typically achieved in routine analyses. Nevertheless, computer simulation is adequate to satisfactorily provide a relative comparison of the effectiveness of different spectral features (single atomic line, multiple atomic lines, single molecular band, all measured spectral lines and bands) for isotopic analysis of uranium, which is one of the main themes of the present paper.

Experimental

Sample and experimental setup

Two sample pellets made from certified U_3O_8 powder (New Brunswick Laboratory, US Department of Energy) with enriched (63.35% ^{235}U, CRM U630) and depleted (0.02% ^{235}U, CRM U0002) uranium isotopes were prepared by pressing about 15 mg of the powder with a 3-mm diameter pellet-pressing die. The U_3O_8 pellets, which were about 300 μm thick, were loaded into a shielded chamber, which contained air at atmospheric pressure, with optical ports for laser ablation and photon collection. Ignoring trace amount of other uranium minor isotopes (i.e., assuming ^{235}U and ^{238}U sum to 100% of all uranium atoms in the CRM), the ratio of ^{235}U:^{238}U in the enriched sample is 64.4:35.6.

The experimental setup consisted of a nanosecond Nd:YAG laser operated at its fundamental wavelength at 1064 nm, a 1.25 m-focal length Czerny-Turner spectrometer (Horiba JY 1250M), and an intensified charge-coupled device (ICCD) gated detector [23]. A pulsed laser, with energy of 40 mJ, was focused onto the sample surface with a fused-silica lens to a spot diameter of approximately 400 μm. Laser-induced plasma emission was collected through another fused-silica lens onto an optical fiber bundle coupled to the spectrometer. Unless otherwise specified, a grating with a groove density

of 2400 lines per mm was used (measured spectral resolution was ~ 18 pm FWHM); the delay time and gate width of the ICCD detector were set at 5 μs and 20 μs, respectively.

Simulation of LIBS and LAMIS spectra

Because databases for spectroscopic constants and isotopic shifts are adequately comprehensive for U atomic lines (U I and U II [11, 12, 24]) but those for molecular UO [25-27] are far from complete, the methods for generating simulated spectra were accordingly different for atomic lines and molecular bands. For simulations involving only atomic emission lines, the simulated spectra were all based on theoretical computation. Published wavelengths from the ^{238}U line list [24] were directly taken for the simulation of the ^{238}U profile, and line positions for the ^{235}U isotope were calculated from the published isotopic shifts [11, 12]. Lorentzian line profiles, with a measured width of 18 pm for emission lines in the 590 nm proximity, were used for the computation of atomic spectra. For the U II 424.437 nm line, a spectral width of 15 pm was used in the simulation because this line can be measured with a 3600 groves/mm grating, in which the cutoff wavelength is 500 nm.

For molecular bands, as will be explained in detail in Section 3.1, the persistence time for UO molecular bands and U atomic lines overlap. In other words, LAMIS spectra for UO bands unavoidably contain some U atomic lines. Since these U lines contain isotopic information of the sample and are inherently present in the LAMIS spectra, a combined LAMIS–LIBS approach was used for isotopic analysis. For the simulation, a set of ^{235}U and ^{238}U base LAMIS–LIBS spectra were obtained from experiments. Because more than 99.98% of uranium in the depleted U_3O_8 sample (CRM U0002) is in the form of ^{238}U, the ^{238}U LAMIS–LIBS base spectrum is taken directly from this depleted U_3O_8 sample. As will be discussed in detail in Section 3.2, the ^{235}U LAMIS–LIBS base spectrum is deduced from the difference between the depleted and enriched (CRM U630) U_3O_8 samples. Once the ^{235}U and ^{238}U base LAMIS–LIBS spectra are determined, simulation of uranium emission spectra at any desired ^{235}U and ^{238}U abundance

173 percentages becomes straightforward through summation of the two U isotopic
174 components.

175 In all cases, emission intensities, signal-to-background ratios, and measurement noise
176 (detector-read, photon-shot and source-flicker) were all experimentally determined and
177 incorporated into the simulation model [10, 22]. For the two U_3O_8 pelletized samples,
178 the measured pulse-to-pulse flicker noise was 14.8% RSD. As the same spectrometric
179 and detector system was used as in our earlier work [10], the previously determined
180 distributions of detector-noise and photon-shot noise were applied in the present study.
181 The detector-read, photon-shot and source-flicker noise levels were independently added
182 to all simulated spectra.

183 Partial least square regression

184 Extraction of isotopic abundance information from the LIBS or LAMIS spectra was
185 achieved with partial least square (PLS) multivariate regression [10, 22]. As PLS
186 regression is a purely empirical approach by matching the emission pattern of the sample
187 with unknown $^{235}U/^{238}U$ ratio to a set of standard reference spectra; it is particularly
188 useful in uranium LAMIS analysis because spectroscopic constants of many rovibronic
189 bands for UO are not documented. In addition, even when the two U isotopic
190 components in the measured spectra are overlapped and resolved only partially, PLS
191 multivariate calibration can be correctly performed [28, 29].

192 In this work, with the exception of the two base spectra from experimental measurements
193 (Section 3.2), all other standards and samples spectra were simulated from these two base
194 profiles. However, the signal and noise behaviors in these simulated spectra should
195 resemble those obtained from experiments, as several noise sources were individually
196 characterized in detail. For ease of discussion and to match typical terminology as in an
197 analysis, from this point onwards, the fact that all spectra of the samples and the
198 standards were simulated will no-longer be repeatedly stressed.

The calibration set consisted of eleven standards with equally spaced ^{235}U abundances from 0% to 100%, whereas the test set contained ten reference samples with ^{235}U abundances evenly distributed between 5% and 95%. The spectra from both the calibration standards and the test samples were each accumulated from 10 laser shots. For each standard, ten replicated spectra were fed into the PLS calibration model. For each test sample, 1000 repeated measurements were made. Assessment of standard deviation requires a large number of samples to be measured, and we have previously [10] shown that 1000 to 3000 measurements is a good compromise between being able to confidently estimate the measurement precision and computation time.

Prior to feeding the spectra into the PLS algorithm, all individual emission spectra were normalized to its norm [29, 30] as a data pre-processing routine to reduce systematic variation and minimize the spectrum uncertainty [29, 31-33]. All spectra simulation and PLS analyses were performed with in-house written LabVIEW programs (LabVIEW 2015, National Instruments). The PLS algorithm used in this study was a PLS1 type and three principal components were utilized in all PLS calibration models [22].

Results and discussion

Identification of U atomic and molecular spectral features

Laser induced plasma emission from uranium is complex in structure as uranium gives rich, and in many cases overlapping, atomic and molecular spectra. For instance, 92,000 U I and U II lines have been observed and were compiled between the wavelength range of 310 to 900 nm [11], which translates to an average of one atomic line in each 6.4-pm spectral window. The UO molecular spectra are even more complex with an average of one molecular *band* in a 1-nm spectral window in the UV-visible range. Kaledin *et al.* [34] reported that approximately 500 UO molecular bands were observed in the emission spectrum in the 400 to 900 nm range with a thermal furnace excitation source operated at 2400 to 2600 K. Although a large number of UO molecular bands have been detected, only a small fraction of those were characterized. The most extensive list on UO

rovibronic levels currently available was published by Kaledin and Heaven [26]; yet, only about fifty UO levels were listed.

A spectral window that contains a strong UO molecular band is selected for this work. Several studies, both experimental [35, 36] and theoretical [27], reported that the most intense UO band is the one that emits at 593.4 nm. Furthermore, it was commented that overlapping of UO bands are particularly marked in the range of 580 to 610 nm [34]. Because PLS regression extracts isotopic information through matching the emission pattern of the sample and the calibration standard, and requires the molecular bands to be resolved only to an extent that there are differences in the spectral features from the two isotopologues, heavily overlapping spectral features could be beneficial as they contain a high density of information. Therefore, the spectral window from 591.6 to 596.5 nm was chosen for the present study. As will be presented below, thirty-two U I lines and three UO bands were positively identified in this comparatively narrow spectral window that spans slightly less than 5 nm.

Emission features from atomic lines or molecular bands can be readily classified through temporally resolved spectra. Figure 1 shows a small section of the measured emission spectra, normalized to the gate width of the ICCD detector, at different delay times, from laser ablation of a depleted U_3O_8 pellet sample. Ionic emission lines (e.g., U II 593.244 and U II 595.205) are strong at early times of the plasma (e.g., 1 μs) but then rapidly decrease to almost baseline level at 5 μs. Neutral-atomic lines (e.g., U I 592.933, U I 593.382, and U I 594.277) resemble ionic lines and show strong emission at early delay times (<1 μs). The major difference is that neutral-atomic lines persist significantly longer, and is one of the two major emitting species at 5 μs delay. Molecular bands (e.g., the UO bands at 593.55, 594.57 and 595.22 nm), in contrast, are relatively weak at early times (<1 μs), but progressively grow and become comparatively strong at longer delay. For example, emission from the UO band at 593.55 nm is only a small fraction to that of the nearby U I 593.382 nm line at 1 μs; the UO band/U I line ratios gradually increase with delay time, and the UO band becomes stronger than the U I line at 5 μs. Temporally

resolved study, as demonstrated in Fig. 1, allows the classification of emission features even for spectra as complex as uranium.

Figure 1 also illustrates two spectral characteristics that would potentially pose impacts on isotopic analysis of uranium by LIBS/LAMIS. First, emission from UO molecular bands and U atomic lines temporally overlap, and it is not practically feasible to select a delay time and detection gate that can measure strong emission from UO bands without U I lines (and vice versa). Therefore, there will be no clear boundary on LIBS (atomic line only) and LAMIS (molecular band only) for U isotopic analysis in laser induced plasmas. Indeed, it is one objective of the present study to understand the potential benefit of including molecular bands to atomic lines for U isotopic analysis. Second, the temporal response of the plasma background appears atypical. Rather than following a monotonically decreasing trend [37], the plasma background initially dropped when the delay time was increased from 1 μs to 2 μs, but then rose at 3 μs and further grew at 5 μs. This rising trend for plasma background at 3 and 5 μs is a result of a pseudo-continuum from the strongly overlapping UO molecular bands. Previous studies [38, 39] also noted intense plasma continuum from a superposition of a multitude of uranium emitting species during laser ablation of metallic uranium samples. An intense pseudo-continuum degrades signal-to-background ratio, and analytical performance could suffer.

Determination of LAMIS–LIBS base spectra for ^{235}U and ^{238}U

For the simulation, a set of ^{235}U and ^{238}U base LAMIS–LIBS spectra were obtained from experiments. Because the two (depleted and enriched) U_3O_8 samples are in the form of pressed pellet housed in separate air-tight chambers, the measured total emission from the two samples was slightly different, probably due to the small variations in the sample properties (e.g., particle size distribution, density and thickness of the pressed pellet) and the reproducibility in positioning the two chambers. Further, our enriched sample contains only ~ 64% ^{235}U. Therefore, a simple model was developed to deduce the base spectrum for 100% ^{235}U from the depleted and enriched U_3O_8 samples, as well as to correct for the slight mismatch in the measured intensities.

The measured spectrum from an U_3O_8 sample (denoted as $I^{measured}(\lambda)$) contains two components – emission from both atomic and molecular species of uranium with the associated pseudo-continuum ($\varepsilon_U(\lambda)$), and true plasma continuum background solely due to ion-electron (either free-free or free-bound) recombination ($\varepsilon_{bkg\text{-}continuum}(\lambda)$).

$$I^{measured}(\lambda) = \varepsilon_U(\lambda) + \varepsilon_{bkg-continuum}(\lambda) \quad (1)$$

It is clear that the U-emission component ($\varepsilon_U(\lambda)$) in the measured spectrum is related to the amount of uranium ablated and present in the plasma (N_U); a U-density normalized emission-signal coefficient ($S_U(\lambda)$), is defined *via* the relation:

$$\varepsilon_U(\lambda) = N_U S_U(\lambda) \quad (2)$$

It is difficult to model the true plasma continuum background component ($\varepsilon_{bkg\text{-}continuum}(\lambda)$) as it involves number densities of ions, electrons and their kinetic temperatures. For the present measurements, the delay time was 5 μs after the laser pulse and the densities of electrons and ions are expected to be low. Hence, the plasma continuum due to ion-electron recombination should be significantly decayed [2, 37]. For example, using a similar setup with an uraninite ore sample but at other wavelengths, we previously reported that the intense plasma continuum emission undergoes rapid decay at 1 μs delay [23]. Although it is expected that the contribution of $\varepsilon_{bkg\text{-}continuum}$ to the total emission is minor, it is included in the derivation of the base profile. Justified by the fact that plasma continuum has been successfully employed as an internal standard for LIBS [40, 41], it can be assumed that $\varepsilon_{bkg\text{-}continuum}$ is directly proportional to N_u (the amount of uranium ablated and present in the plasma) through the U-density normalized background coefficient ($B_U(\lambda)$). Furthermore, we assume that this normalized background coefficient ($B_U(\lambda)$) is identical for ^{235}U and ^{238}U in the laser plasma.

$$\varepsilon_{bkg-continuum}(\lambda) = N_U B_U(\lambda) \quad (3)$$

The experimentally measured emission spectrum (Equation 1) can be re-written as

$$I^{measured}(\lambda) = N_U\big(S_U(\lambda) + B_U(\lambda)\big) \tag{4}$$

The term ($S_U(\lambda) + B_U(\lambda)$) represents the base spectrum, which is the spectrum normalized to the amount of ablated material in the plasma. The base spectrum can be conveniently obtained through normalization of the measured spectrum with its total intensity (i.e., area under the spectrum). The normalization effectively compensates the slight mismatch in ablation efficiencies of the two samples. Because more than 99.98% of the uranium is in the form of ^{238}U in the depleted U_3O_8 sample, the base spectrum for ^{238}U, ($S_{U\text{-}238} + B_U$), is simply the measured spectrum from the depleted sample after normalization with its total intensity.

$$\big(S_{U-238}(\lambda) + B_U(\lambda)\big) = \frac{I^{measured}_{depleted-U}(\lambda)}{\sum I^{measured}_{depleted-U}(\lambda)} \tag{5}$$

The procedure to obtain the base spectrum for ^{235}U, ($S_{U\text{-}235} + B_U$), is slightly more complicated because the ^{235}U:^{238}U ratio in the enriched U_3O_8 sample is only 64.4:35.6. Measured emission for the enriched sample, therefore, is

$$\begin{aligned} I^{measured}_{enriched-U}(\lambda) &= N_{enriched-U}\big(S_{enriched-U}(\lambda) + B_U(\lambda)\big) \\ &= N_{enriched-U}\big[0.64\big(S_{U-235}(\lambda) + B_U(\lambda)\big) \\ &\quad + 0.36\big(S_{U-238}(\lambda) + B_U(\lambda)\big)\big] \end{aligned} \tag{6}$$

After rearrangement and with Equation 5, the base spectrum for ^{235}U, ($S_{U\text{-}235} + B_U$), can be obtained from the total intensity-normalized spectrum of the enriched and depleted sample through

$$\begin{aligned} \big(S_{U-235}(\lambda) + B_U(\lambda)\big) &= \frac{1}{0.64}\left[\frac{I^{measured}_{enriched-U}(\lambda)}{\sum I^{measured}_{enriched-U}(\lambda)} - 0.36\big(S_{U-238}(\lambda) + B_U(\lambda)\big)\right] \\ &= \frac{1}{0.64}\left[\frac{I^{measured}_{enriched-U}(\lambda)}{\sum I^{measured}_{enriched-U}(\lambda)} - 0.36\,\frac{I^{measured}_{depleted-U}(\lambda)}{\sum I^{measured}_{depleted-U}(\lambda)}\right] \end{aligned} \tag{7}$$

With Equations 5 and 7, base profiles for both ^{235}U and ^{238}U were obtained from the measured spectra of the enriched and depleted U samples. Several atomic lines and

molecular bands were found to exhibit distinct isotope shifts, and some of these spectral features are presented in Figs. 2a and 2b.

The strongest UO band at 593.55 nm with its neighboring U I line at 593.382 nm are shown in Fig. 2a. In this manuscript, all wavelengths are referenced to the ^{238}U isotope. The ^{235}U isotope shift for the U I line is +8.5 pm (i.e., towards the red) whereas the shift for the peak of the UO band is ~ –35 pm (i.e., a blue shift). The isotopic shift for the UO band is only a few times larger than that of the U I line, partly due to the exceptionally large isotopic shift for U atomic lines as mentioned in the introduction, and partly because the reduced mass of UO molecule is dominated by the much lighter O atom and hence is only slightly altered when the U atom is changed from ^{238}U to ^{235}U. Based solely on the magnitude of its isotope shift, the UO band might not look particularly attractive for isotopic analysis. However, the substantial perturbations in the UO molecular energy levels [36, 42] provide some additional unique spectral features that can be exploited for isotopic analysis. To elaborate, because of the large number of electronic states available and the high degree of configuration mixing present in uranium, perturbations in U-bearing molecular energy levels are heavy and frequent [42-44]. Heaven *et al.* [42] and Kaledin *et al.* [25, 26] found that many UO bands are perturbed to a degree that prevented rotational analysis. Because the extent of perturbations depends on the specific interactions and mixing of the energy levels, which is isotope dependent, it has been reported that perturbations in UO are different for its isotopologues [43] and the effect of isotopic substitution on the spectrum is so profound that the correlation between bands for the two species cannot be made with any confidence [42]. These isotope-specific perturbations in UO bring not only abnormally large isotopic shifts than those predicted from a classical reduced-mass formula in molecular spectroscopy, but also change the spectral intensity and pattern [42]. For example, Heaven *et al.* [42] reported that $U^{16}O$ has only one intense feature in the 17450–17700 cm^{-1} spectral region but $U^{18}O$ shows two strong features in this region with intensities differing by a factor of six. The dramatic change in spectral pattern by isotopic substitution in UO provides a beneficial feature for isotopic analysis.

Figure 2b shows a small section of the LIBS and LAMIS spectra from 594.25 to 595.25 nm for ^{235}U and ^{238}U. In this 1-nm spectral window, six U I lines and two UO bands were identified. The wavelengths of the two identified UO bands match those listed by Kaledin and Heaven [26]. Both UO bands exhibit dissimilar spectral patterns for the two isotopologues, and their differences are more than merely simple wavelength shifts. These differences can be readily extracted by the PLS regression calibration and utilized for isotopic analysis.

Simulation of U isotopic analysis by LAMIS with only one UO band at 593.55 nm

To simulate the analytical performance of LAMIS with a single UO molecular band, the most intense band at 593.55 nm was chosen. The simulation was comprised of isotopic determination of ten simulated reference samples with ^{235}U abundances evenly distributed between 5% and 95%. Spectral features from 593.424 to 593.849 nm in the experimentally determined spectra (cf. the marked region in Fig. 2a) were used as base profiles for this single-band LAMIS simulation. Figure 3 shows the difference between predicted and true values (left axis) and predicted ^{235}U isotopic abundances (right axis) against the ^{235}U isotopic abundances in the sample. Because the calibration standards and the samples in the simulation model were obtained through *linear* combinations of the two ^{235}U and ^{238}U base profiles, the addition of noise affects only precision and no bias is expected from the PLS model (cf. Fig. 3). The absolute precisions were about 1.5% for all studied ^{235}U abundances. Furthermore, in simulations with other spectral features (e.g., single atomic line, pool of multiple atomic lines, combined LAMIS–LIBS) to be discussed below, it was found that all precisions were independent of the ^{235}U abundances. Therefore, it is a more straightforward approach to evaluate and compare the performance through averaged precision of all the test samples, which is defined as $\sqrt{\frac{1}{N}\sum(C_{pred} - C_{true})^2}$. Because there is no expected bias, the differences between the predicted (denoted by C_{pred}) and the standard (C_{true}) isotopic abundances reflect only precision. The averaged precision of all the ten test samples presented in Fig. 3 is 1.49% in absolute ^{235}U abundances.

Simulation of U isotopic analysis by LIBS with U lines in-between 591.6 and 596.5 nm

The analytical performances of pure U atomic lines (i.e., without contributions from molecular bands) in the spectral window from 591.6 to 596.5 nm also were simulated. The results were compared to those with the contributions from molecular bands in the same spectral window to be presented in the next section. Unlike the case with molecular band, in which base spectra for ^{235}U and ^{238}U were obtained experimentally (cf. Figs. 2a and 2b), simulated emission spectra for *pure* atomic lines were theoretically computed from a published line list [24] and isotopic shifts [11] to ensure that the simulation results represent the case when only atomic-line spectral features are used in the isotopic analysis.

If the analysis is limited to a single atomic line, the strongest emission line should be used providing that its isotopic shift is adequate. Our previous results [10] showed that the quality of isotopic analyses of U by LIBS generally are dependent on the signal-to-background ratio (SBR) and net intensity of the emission line, rather than the magnitude of isotopic shifts. Accordingly, the strongest U I line at 593.382 nm was selected for single-line analysis (cf. Fig. 2a). The experimentally measured SBR for this U I line was 0.43. The averaged simulated precision from the ten test samples is 1.62% in absolute ^{235}U abundances, which is only slightly degraded from the case of a single UO band. The SBRs of the U I 593.382 nm line and the UO 593.55 nm band are very similar (cf. Fig. 2a) whereas their isotopic shifts are 8.5 pm and 35 pm, respectively; yet, their simulated precisions are very comparable, which is in agreement with our previous findings [10].

The simulation was further extended to multiple atomic-line analysis. All U I lines between 591.6 and 596.5 nm documented in the extensive line list by Palmer *et al.* [24] were included. This spectral window matches that captured by a single ICCD exposure with our spectrometer-detector system. Emission intensities reported by Palmer *et al.* [24] were from a hollow cathode discharge with an electronic excitation temperature

around 4400 K, and can be readily transformed to other temperatures (e.g., the temperature of our LIBS plasma). Table 1 lists the spectroscopic constants [45] of the three U I lines used to determine the excitation temperature of our LIBS plasma. Linear regression (with $R^2 > 0.98$) of the Boltzmann plot gave an excitation temperature of 5300 K. The uncertainty in the slope of the Boltzmann plot was 10%. Table 2 lists the wavelengths, ^{235}U–^{238}U isotope shifts, upper energy levels, and rescaled relative intensities to a temperature of 5300 K of the thirty-two U I lines used in the multiple-line simulation. Figure 4 shows the experimentally measured ^{238}U LAMIS–LIBS (molecular bands together with atomic lines) spectrum and the simulated U I lines (before addition of plasma continuum background and simulated measurement noise). Overall, the pattern of the simulated U I lines matches well with those from measurement. Those spectral features in the LAMIS–LIBS experimental spectrum that are not covered by the simulated U I profile likely originate from UO molecular bands.

In this multiple atomic-line simulation, the SBR of the U I 593.382 nm line was kept 0.43 (i.e., identical to the single line case) and emission of other U I lines were then varied according to the predefined relative intensities listed in Table 2. The use of multiple emission lines brings a significant improvement in the analytical performance compared to the use of single atomic line or UO band. The averaged precision from the ten test samples lowers to 0.72%.

Simulation of U isotopic analysis by LAMIS–LIBS combined approach

As mentioned earlier, there are temporal overlaps in the UO molecular bands and U atomic lines. These spectral features (LAMIS and LIBS) can be used together for the isotopic analysis. Experimentally measured LAMIS–LIBS base profiles for ^{235}U and ^{238}U (cf. Figs. 2a and 2b), were used in the simulation. The spectral window was the same as in the case of multiple atomic lines simulation (i.e., between 591.6 and 596.5 nm). Figure 5 summarizes the averaged precision of ^{235}U isotopic abundance for different combinations of spectral features incorporated into the analysis. Compared to the use of only atomic lines (LIBS with a collection of multiple lines), the inclusion of

multiple UO molecular bands in the analysis further improve the precision from 0.72% to 0.42%. These results clearly show that although many of the molecular features are faint and appear noisy (many of them are with SBR $\leq$ 0.1, cf. Fig. 4), useful isotopic information about the sample can be extracted when sufficient large amount of weak spectral features are present.

Simulation of U isotopic analysis by LIBS with U II 424.437 nm

The last simulation performed in this study is to compare the analytical performance of LAMIS–LIBS combined approach in the 595 nm proximity to single emission-line analysis with the U II 424.437 nm benchmark. This U II line was commonly used for uranium isotopic analysis particularly with atomic emission [14, 46-50]. Simulation shows that its averaged precision is 0.48% in absolute ^{235}U abundances, a notable value for single-line analysis. The measured SBR for the strongest spectral features in the LAMIS–LIBS spectrum (cf. Fig. 4) was only ~ 0.4, whereas the SBR for the U II 424.437 nm line was substantially larger and was 1.38. As the flat component of plasma background contains no extractable information but brings photon-shot noise, the analytical performance of the LAMIS–LIBS combined analysis from a collection of molecular bands and atomic lines is only similar to single-line analysis with the benchmark U II line (cf. Fig. 5). Nevertheless, the LAMIS–LIBS combined approach shows its potential as a viable supplement and valuable alternative for U isotopic analysis in situation that the single U II 424.437 nm line suffers interference and cannot be utilized. Because analyte signals (LIBS or LAMIS) are highly correlated, the use of multiple spectral features as in the LAMIS–LIBS approach provides the necessary resource for the PLS algorithm to differentiate the spectral patterns from the analyte against those from spectral interferences [22] – an attribute that would be difficult to implement if only a single spectral component (e.g., one atomic emission line) is used.

Conclusions

Isotopic analysis through the use of molecular spectrometry for the heaviest naturally occurring element – uranium – was presented in this work. Spectral features and characteristics of isotopic shifts for UO were identified. Through computer simulation, the theoretical precisions attainable by LAMIS, LIBS and LAMIS–LIBS combined approach for uranium isotopic analysis were studied. The analytical performance of LAMIS with the most intense UO band at 593.4 nm (averaged simulated precision 1.5%) was found to be slightly better than the use of a nearby single U I line (precision 1.6%) with similar intensity but significantly smaller isotopic shift. The use of multiple (a total of thirty-two) atomic emission lines improves the precision to 0.72%. Despite the fact that many UO spectral characteristics appear weak (many with SBR $\leq$0.1 due to intense pseudo-continuum background), further inclusion of the molecular spectral features to the multiple atomic lines (i.e., the LAMIS–LIBS combined approach) advances the precision to 0.42%. Analytical performances of the LAMIS–LIBS combined approach compares well with the U II 424.437 nm benchmark (precision 0.48%), and thus shows its potential as a viable and valuable alternative for U isotopic analysis in situations that the benchmark U II line cannot be used. The present study offers a better understanding on the analytical performance of isotopic analysis with LAMIS and LIBS for uranium, in which its spectral features (in particular its molecular spectroscopy) are complex, generally unresolved and largely uncharacterized.

Acknowledgements

This work was supported by the Defense Nuclear Nonproliferation Research and Development Office and the Office of Basic Energy Sciences of the U.S. Department of Energy under contract number DE-AC02-05CH11231 at the Lawrence Berkeley National Laboratory.

References

1. Mao X, Bol'shakov AA, Choi I, McKay CP, Perry DL, Sorkhabi O, Russo RE (2011) Laser ablation molecular isotopic spectrometry: Strontium and its isotopes. Spectrochim Acta Part B 66 (11–12):767-775
2. Mao X, Bol'shakov AA, Perry DL, Sorkhabi O, Russo RE (2011) Laser ablation molecular isotopic spectrometry: Parameter influence on boron isotope measurements. Spectrochim Acta Part B 66 (8):604-609
3. Russo RE, Bol'shakov AA, Mao X, McKay CP, Perry DL, Sorkhabi O (2011) Laser ablation molecular isotopic spectrometry. Spectrochim Acta Part B 66 (2):99-104
4. Sarkar A, Mao X, Chan GCY, Russo RE (2013) Laser ablation molecular isotopic spectrometry of water for $_1D^2/_1H^1$ ratio analysis. Spectrochim Acta Part B 88:46-53
5. Hou H, Chan GCY, Mao X, Zorba V, Zheng R, Russo RE (2015) Femtosecond laser ablation molecular isotopic spectrometry for zirconium isotope analysis. Anal Chem 87 (9):4788-4796
6. Bol′shakov AA, Mao X, Jain J, McIntyre DL, Russo RE (2015) Laser ablation molecular isotopic spectrometry of carbon isotopes. Spectrochim Acta Part B 113:106-112
7. Wiese WL, Fuhr JR (2009) Accurate atomic transition probabilities for hydrogen, helium, and lithium. J Phys Chem Ref Data 38 (3):565-565
8. King WH (1984) Isotopic shifts in atomic spectra. 1st edn. Plenum Press, New York
9. Hertel IV, Schulz C-P (2015) Hyperfine structure. In: Hertel IV, Schulz C-P (eds) Atoms, molecules and optical physics 1: Atoms and spectroscopy. 1st. edn. Springer Berlin Heidelberg, Berlin, Heidelberg, pp 447-493
10. Chan GCY, Mao X, Choi I, Sarkar A, Lam OP, Shuh DK, Russo RE (2013) Multiple emission line analysis for improved isotopic determination of uranium – a computer simulation study. Spectrochim Acta Part B 89:40-49
11. Blaise J, Radziemski LJ (1976) Energy-levels of neutral atomic uranium (U I). J Opt Soc Am 66 (7):644-659
12. Blaise J, Wyart JF, Verges J, Engleman R, Palmer BA, Radziemski LJ (1994) Energy-levels and isotope shifts for singly ionized uranium (U II). J Opt Soc Am B 11 (10):1897-1929

13. Cremers DA, Beddingfield A, Smithwick R, Chinni RC, Jones CR, Beardsley B, Karch L (2012) Monitoring uranium, hydrogen, and lithium and their isotopes using a compact laser-induced breakdown spectroscopy (LIBS) probe and high-resolution spectrometer. Appl Spectrosc 66 (3):250-261
14. Doucet FR, Lithgow G, Kosierb R, Bouchard P, Sabsabi M (2011) Determination of isotope ratios using laser-induced breakdown spectroscopy in ambient air at atmospheric pressure for nuclear forensics. J Anal At Spectrom 26 (3):536-541
15. D'Ulivo A, Onor M, Pitzalis E, Spiniello R, Lampugnani L, Cristoforetti G, Legnaioli S, Palleschi V, Salvetti A, Tognoni E (2006) Determination of the deuterium/hydrogen ratio in gas reaction products by laser-induced breakdown spectroscopy. Spectrochim Acta Part B 61 (7):797-802
16. Suyanto H, Lie ZS, Niki H, Kagawa K, Fukumoto K, Rinda H, Abdulmadjid SN, Marpaung AM, Pardede M, Suliyanti MM, Hidayah AN, Jobiliong E, Lie TJ, Tjia MO, Kurniawan KH (2012) Quantitative analysis of deuterium in zircaloy using double-pulse laser-induced breakdown spectrometry (LIBS) and helium gas plasma without a sample chamber. Anal Chem 84 (5):2224-2231
17. Morgan PK, Scott JR, Jovanovic I (2016) Hybrid interferometric/dispersive atomic spectroscopy of laser-induced uranium plasma. Spectrochim Acta Part B 116:58-62
18. Chan GCY, Choi I, Mao X, Zorba V, Lam OP, Shuh DK, Russo RE (2016) Isotopic determination of uranium in soil by laser induced breakdown spectroscopy. Spectrochim Acta Part B 122:31-39
19. Smith CA, Martinez MA, Veirs DK, Cremers DA (2002) Pu-239/Pu-240 isotope ratios determined using high resolution emission spectroscopy in a laser-induced plasma. Spectrochim Acta Part B 57 (5):929-937
20. Hou H, Chan GCY, Mao X, Zheng R, Zorba V, Russo RE (2015) Femtosecond filament-laser ablation molecular isotopic spectrometry. Spectrochim Acta Part B 113:113-118
21. Konjevic N (1999) Plasma broadening and shifting of non-hydrogenic spectral lines: Present status and applications. Phys Rep 316 (6):339-401
22. Mao X, Chan GCY, Zorba V, Russo RE (2016) Reduction of spectral interferences and noise effects in laser ablation molecular isotopic spectrometry with partial least

square regression – a computer simulation study. Spectrochim Acta Part B 122:75-84

23. Choi I, Chan GCY, Mao X, Perry DL, Russo RE (2013) Line selection and parameter optimization for trace analysis of uranium in glass matrices by laser-induced breakdown spectroscopy (LIBS). Appl Spectrosc 67 (11):1275-1284
24. Palmer BA, Engleman RJ, Keller RA (1980) An atlas of uranium emission intensities in a hollow-cathode discharge (LA-8251-MS), Los Alamos National Laboratory
25. Kaledin LA, McCord JE, Heaven MC (1994) Laser spectroscopy of UO: Characterization and assignment of states in the 0 to 3 eV range, with a comparison to the electronic structure of ThO. J Mol Spectrosc 164 (1):27-65
26. Kaledin LA, Heaven MC (1997) Electronic spectroscopy of UO. J Mol Spectrosc 185 (1):1-7
27. Tyagi R, Zhang Z, Pitzer RM (2014) Electronic spectrum of the UO and UO^+ molecules. J Chem Phys A 118 (50):11758-11767
28. Zolfonoun E, Ahmadi SJ (2013) Application of multivariate curve resolution-alternating least squares for the determination of boron isotope ratios by inductively coupled plasma-optical emission spectrometry. Spectrochim Acta Part B 81:64-68
29. Sarkar A, Mao X, Russo RE (2014) Advancing the analytical capabilities of laser ablation molecular isotopic spectrometry for boron isotopic analysis. Spectrochim Acta Part B 92:42-50
30. Sarkar A, Karki V, Aggarwal SK, Maurya GS, Kumar R, Rai AK, Mao X, Russo RE (2015) Evaluation of the prediction precision capability of partial least squares regression approach for analysis of high alloy steel by laser induced breakdown spectroscopy. Spectrochim Acta Part B 108:8-14
31. Zeaiter M, Roger JM, Bellon-Maurel V (2005) Robustness of models developed by multivariate calibration. Part II: The influence of pre-processing methods. Trends Anal Chem 24 (5):437-445
32. Feng J, Wang Z, West L, Li Z, Ni W (2011) A PLS model based on dominant factor for coal analysis using laser-induced breakdown spectroscopy. Anal Bioanal Chem 400 (10):3261-3271

33. Feilhauer H, Asner GP, Martin RE, Schmidtlein S (2010) Brightness-normalized partial least squares regression for hyperspectral data. J Quant Spectrosc Radiat Transf 111 (12-13):1947-1957
34. Kaledin LA, Shenyavskaya EA, Gurvich LV (1986) The electronic spectrum of the uranium monoxide molecule. Russ J Phys Chem 60 (4):633-635
35. Kaledin LA, Kulikov AN, Kobylyanskii AL, Shenyavskaya EA, Gurvich LV (1987) The relative positions of the low-lying states of the uranium monoxide (UO) molecule. Russ J Phys Chem 61 (5):712-714
36. Dmitriev YN, Kaledin LA, Kobyliansky AI, Kulikov AN, Shenyavskaya EA, Gurvich LV (1987) Electronic spectra of diatomic molecules containing *f*-elements: GdO, EuF and UO. Acta Physica Hungarica 61 (1):51-54
37. Fisher BT, Johnsen HA, Buckley SG, Hahn DW (2001) Temporal gating for the optimization of laser-induced breakdown spectroscopy detection and analysis of toxic metals. Appl Spectrosc 55 (10):1312-1319
38. Zhang D, Ma X, Wang S, Zhu X (2015) Influence of ambient gas on laser-induced breakdown spectroscopy of uranium metal. Plasma Sci Technol 17 (11):971-974
39. Emmert LA, Chinni RC, Cremers DA, Jones CR, Rudolph W (2011) Comparative study of femtosecond and nanosecond laser-induced breakdown spectroscopy of depleted uranium. Appl Opt 50 (3):313-317
40. Lazic V, Fantoni R, Colao F, Santagata A, Morone A, Spizzichino V (2004) Quantitative laser induced breakdown spectroscopy analysis of ancient marbles and corrections for the variability of plasma parameters and of ablation rate. J Anal At Spectrom 19 (4):429-436
41. St-Onge L, Kwong E, Sabsabi M, Vadas EB (2002) Quantitative analysis of pharmaceutical products by laser-induced breakdown spectroscopy. Spectrochim Acta Part B 57 (7):1131-1140
42. Heaven MC, Nicolai JP, Riley SJ, Parks EK (1985) Rotationally resolved electronic spectra for uranium monoxide. Chem Phys Lett 119 (2-3):229-233
43. Heaven MC (2006) Probing actinide electronic structure using fluorescence and multi-photon ionization spectroscopy. Phys Chem Chem Phys 8 (39):4497-4509

44. Heaven MC, Barker BJ, Antonov IO (2014) Spectroscopy and structure of the simplest actinide bonds. J Chem Phys A 118 (46):10867-10881
45. Corliss CH (1976) Line strengths and lifetimes of levels in neutral uranium. J Res Nat Bur Stand Sec A 80 (1):1-7
46. Saunderson JL (1960) A method of uranium isotope analysis by direct reading emission spectroscopy. Talanta 6:63-70
47. Leys JA, Perkins RE (1966) Uranium isotope analysis by optical emission spectrometry. Anal Chem 38 (8):1099-1101
48. Krachler M, Carbol P (2011) Validation of isotopic analysis of depleted, natural and enriched uranium using high resolution ICP-OES. J Anal At Spectrom 26 (2):293-299
49. Edelson MC, Fassel VA (1981) Isotopic abundance determinations by inductively coupled plasma atomic emission spectroscopy. Anal Chem 53 (14):2345-2347
50. Pietsch W, Petit A, Briand A (1998) Isotope ratio determination of uranium by optical emission spectroscopy on a laser-produced plasma - basic investigations and analytical results. Spectrochim Acta Part B 53 (5):751-761

625 **Table 1** Spectroscopic constants of the three U I lines used in the determination of
626 electronic excitation temperature of the LIBS plasma [45]

Wavelength (nm)	E_{lower} (cm^{-1})	E_{upper} (cm^{-1})	gA (s^{-1})
593.382	620	17468	2.8×10^6
594.277	5762	22584	5.8×10^6
594.857	7646	24452	1.2×10^7

627

Table 2 List of U I emission lines between 591.6 and 596.5 nm. Emission wavelengths for ^{238}U and their upper energy levels are taken from Palmer *et al.* [24] Isotopic shift (IS) data are calculated from the list published by Blaise and Radziemski [11]; a negative sign indicates that the ^{235}U wavelength is lower (i.e., blue shifted) than that of ^{238}U. Relative intensity is calculated based on the emission intensity given by Palmer *et al.* [24] for a hollow cathode discharge at 4400 K and rescaled to 5300 K through Boltzmann distribution.

^{238}U Wavelength (nm)	^{235}U–^{238}U IS (pm)	E_{upper} (cm^{-1})	Relative intensity at 5300 K
591.9252	-9.63	28566	0.1118
591.9667	-10.16	23908	0.2338
592.2899	-10.52	27133	0.0585
592.3654	-23.86	28184	0.1960
592.3732	1.05	21329	0.1844
592.5316	-7.20	22634	0.1679
592.5455	7.20	24517	0.8746
592.9318	-17.93	20661	0.5754
592.9667	-12.48	24185	0.1245
592.9753	-12.48	27148	0.1225
593.3818	8.45	17468	1.0000
593.4844	Unknown*	29488	0.1162
593.5508	-10.57	23848	0.1408
593.7373	-8.11	27394	0.1462
593.9991	-9.17	24022	0.2414
594.0664	10.06	28285	0.1083
594.2769	-3.71	22584	0.5745
594.3412	25.08	23069	0.1760
594.7672	17.16	23057	0.3408
594.8170	-7.78	24940	0.0892
594.8566	-0.89	24451	0.7934

594.9662	-5.13	21078	0.3830
595.3650	-4.96	27477	0.0654
595.4372	-1.77	27475	0.1230
595.4673	4.96	26997	0.0597
595.4899	6.56	24906	0.2396
595.5620	-12.95	24650	0.0493
595.6812	-5.14	28341	0.0627
595.6859	-12.07	20651	0.8370
595.9944	-11.90	28451	0.1663
596.1901	-27.37	31270	0.0967
596.3940	-15.47	28053	0.1121

*isotopic shift for this line is unknown and is assumed to be zero (i.e., same wavelengths for ^{235}U and ^{238}U) in the simulation.

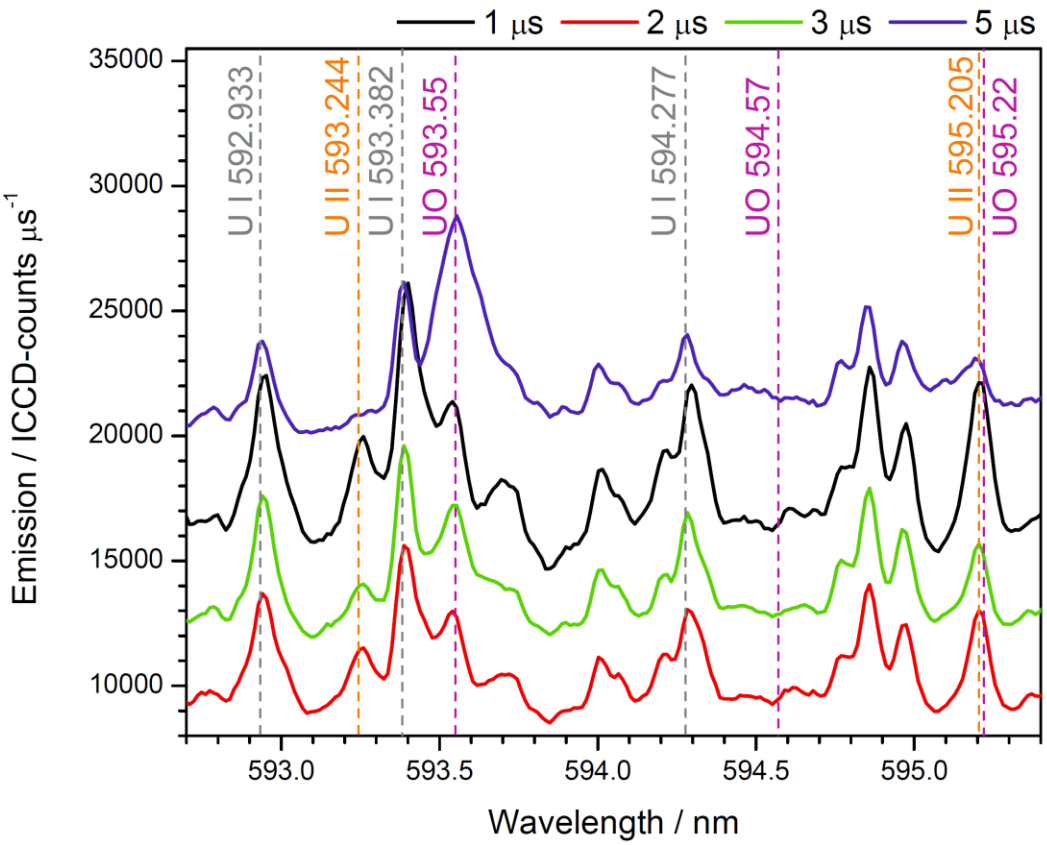

638

639 **Fig. 1** Temporally resolved emission spectra at different ICCD delays from a depleted
640 U_3O_8 pelletized sample. The ICCD gate widths were 1, 1, 2 and 4 μs,
641 respectively, for delays 1, 2, 3 and 5 μs. All emission is normalized to the gate
642 width of the ICCD detector. A lower-resolution grating (1200 grooves/mm) was
643 used for this spectral survey. The nominal wavelengths for atomic lines are
644 referenced to ^{238}U

645

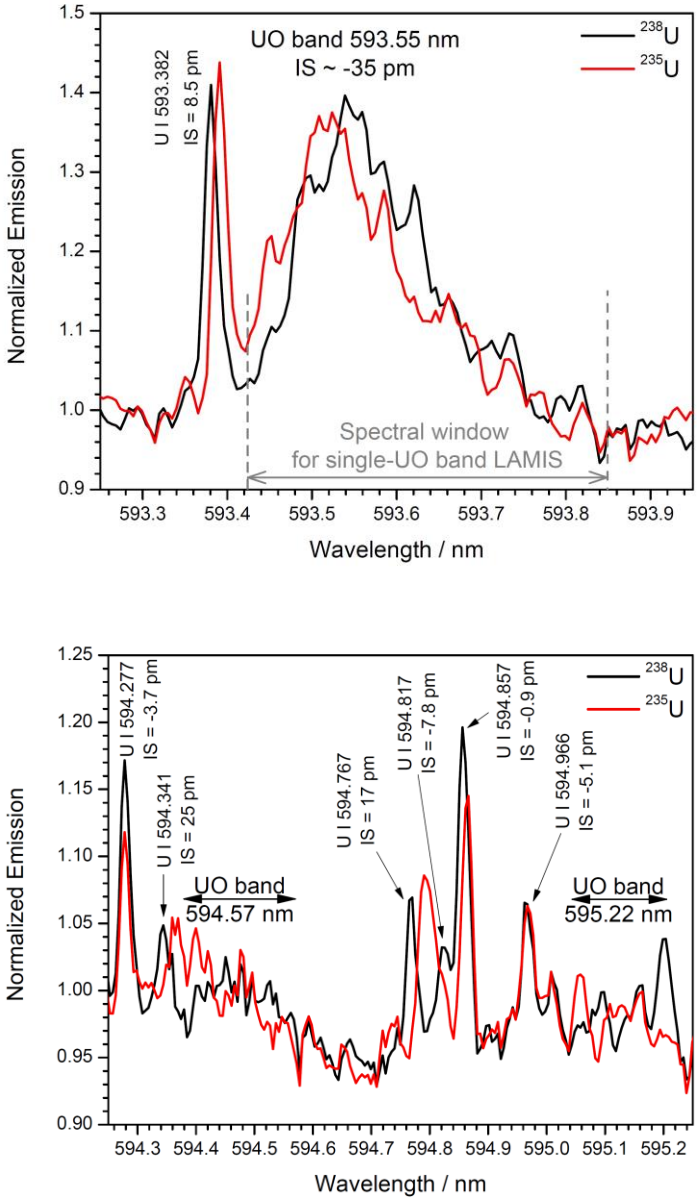

Fig. 2 ^{235}U and ^{238}U base spectral profiles of some selected atomic lines and molecular bands exhibiting distinct isotopic shifts. (a, top) The intense UO band at 593.55 nm and its neighboring U I line at 593.382 nm (with their isotopic shifts). The marked region shows the base profiles used in the single UO-band LAMIS simulation. (b, bottom) A 1-nm window from 594.25 to 595.25 nm showing different emission patterns, in addition to isotopic shifts, of two UO bands. All spectra were recorded with a 2400 grooves/mm grating. The nominal wavelengths for atomic lines are referenced to ^{238}U

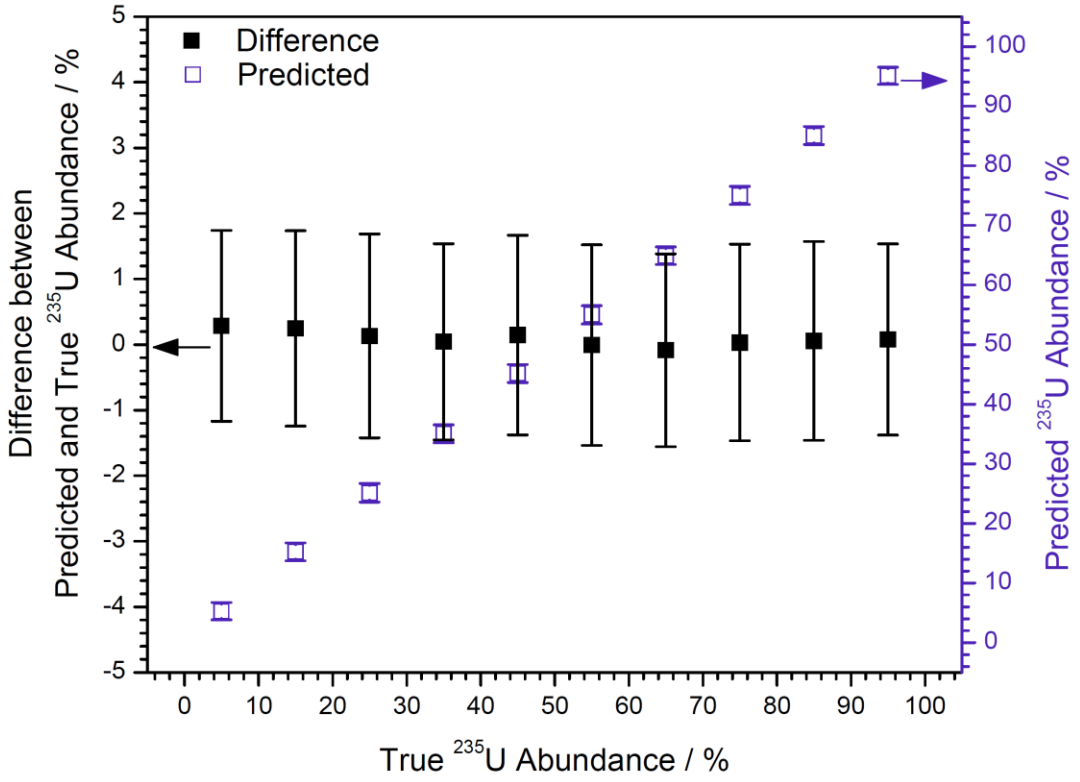

Fig. 3 Analytical bias and precision (left axis) and determined isotopic abundances of ^{235}U (right axis) against known ^{235}U abundances in the simulation. The calibration set contained eleven standards with equally spaced ^{235}U abundances from 0% to 100%. All simulated spectra (both the samples and the calibration standards) were accumulated from 10 laser shots

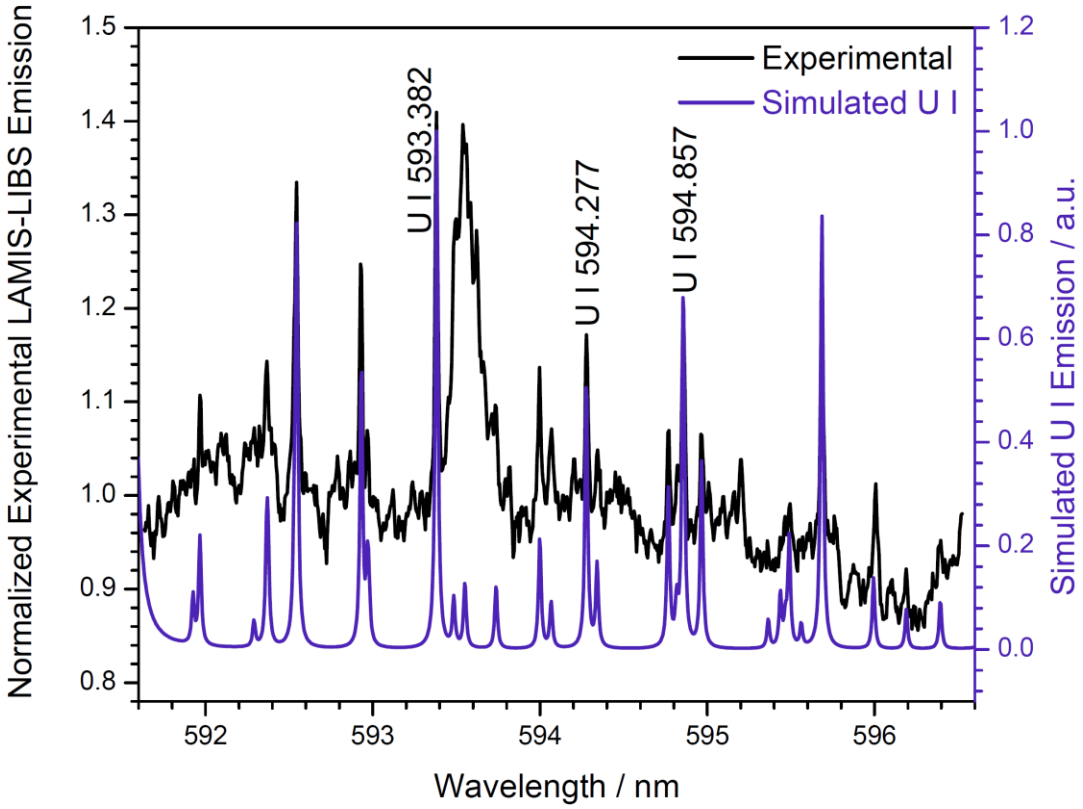

664

665 **Fig. 4** Experimentally measured ^{238}U LAMIS–LIBS (molecular bands together with
666 atomic lines) spectrum, and the simulated U I lines with an electronic excitation
667 temperature of 5300 K. The three labelled U I lines are those employed in the
668 Boltzmann plot for the evaluation of excitation temperature. The experimental
669 spectrum was recorded with a depleted U_3O_8 sample and a 2400 grooves/mm
670 grating

671

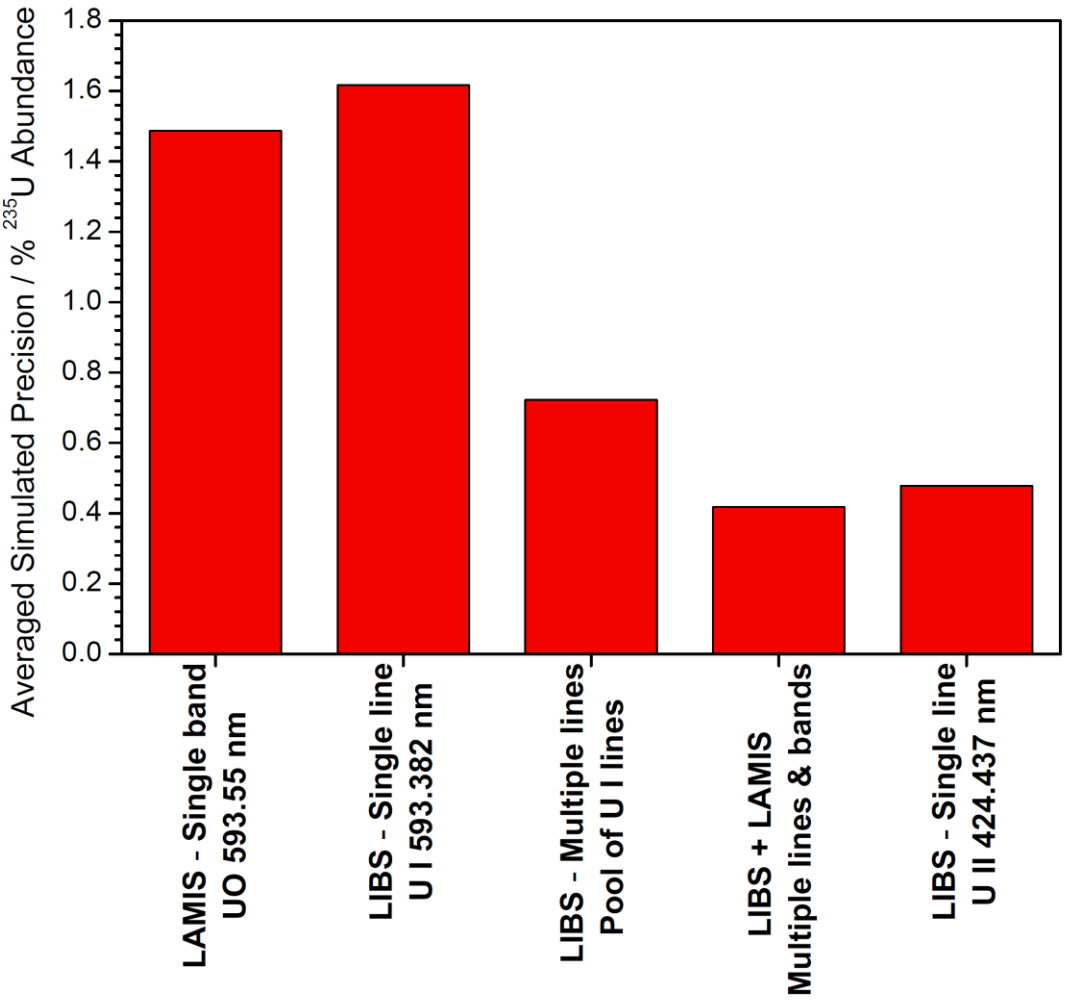

672

673 **Fig. 5** Averaged simulated precision (in percentage ^{235}U abundance) when different
674 atomic and molecular spectral features are incorporated into the PLS calibration
675 model

676